

Holographic metals at finite volume

Lucas Acito, Nicolás Grandi,

*Instituto de Física La Plata (IFLP), CONICET &
Departamento de Física Dr. Emil H. Bose, UNLP
C.C. 67, (1900) La Plata, Argentina.*

E-mail: acitolucas@gmail.com, grandi@fisica.unlp.edu.ar

ABSTRACT: We construct the electron star solution in asymptotically global AdS space-time, and investigate its stability properties, both locally under perturbations and globally with respect to the Reissner-Nordström black hole and thermal AdS metrics. We interpret the resulting phase diagram as that of a holographic metal confined to a finite volume. We identify a quantum critical point at finite chemical potential, around which the different phases are organized.

Contents

1	Introduction	1
2	The model	2
3	Solutions: black hole and electron star	5
4	Phase Transitions	8
5	Discussion and future directions	10
6	Acknowledgements	11
A	Details of the model	12
B	Free energy computation details	15
C	Black hole surrounded by an electron cloud	19

1 Introduction

One of the most interesting applications of holography during the past decade is that of the description of strongly coupled condensed matter systems. In this context, there has been a lot of activity regarding the properties of the superconducting [1–3] and metallic [4–7] phases from the holographic perspective.

A central property of the holographic duality is that the boundary field theory is conformal. This implies that, in constructing the phase diagram, one of its thermodynamic quantities (say the chemical potential μ) would play the role of setting the overall scale, leaving the others (say the temperature T and the magnetic field B) as the independent dimensions of the phase diagram (in the example, those would be T/μ and B/μ). This contrasts with the real High T_c materials, which have a intrinsic dimensionful parameter a that sets the scale in the phase diagram (like T/a , B/a and μ/a).

To our knowledge, two possible paths have been proposed in the literature which overcome the aforementioned limitation. One is to include an additional bulk field whose boundary value defines the scale a [8] (see also [9, 10]). This faces us to the new problem of finding a sensible physical interpretation for the new degree of freedom from the boundary point of view. The other proposal is to abandon the planar setup used in most of the investigations in the subject, in favor of a spherical boundary [11] (see also [12, 13]). In this case, the boundary curvature radius plays the role of a .

It is the aim of this work to investigate the temperature T/a versus chemical potential μ/a phase diagram of the electron star with a spherical boundary, whose holographic interpretation is that of a metallic phase contained inside a spherical vessel.

2 The model

We consider the dynamics of a charged perfect fluid coupled to the gravitational and electromagnetic fields in $3+1$ dimensions, for details see Appendix A. The relevant degrees of freedom are the metric $g_{\mu\nu}$, the electromagnetic field A_μ and the fluid four-velocity u^μ . The equations of motion take the form

$$R_{\mu\nu} - \frac{1}{2}g_{\mu\nu} - \frac{3}{L^2}g_{\mu\nu} = \kappa^2 \left(T_{\mu\nu}^{\text{EM}} + T_{\mu\nu}^{\text{Fluid}} \right) \quad \nabla_\mu F^{\nu\mu} = e^2 J^\nu \quad (2.1)$$

with $T_{\mu\nu}^{\text{EM}}$ and $T_{\mu\nu}^{\text{Fluid}}$ are the electromagnetic and fluid energy momentum tensors respectively, and J^μ is the electric current

$$\begin{aligned} T_{\mu\nu}^{\text{EM}} &= \frac{1}{e^2} \left(F_{\mu\alpha} F_\nu^\alpha - \frac{1}{4} g_{\mu\nu} F_{\alpha\beta} F^{\alpha\beta} \right) & J^\mu &= \sigma u^\mu \\ T_{\mu\nu}^{\text{Fluid}} &= g_{\mu\nu} P + (\rho + P) u_\mu u_\nu \end{aligned} \quad (2.2)$$

This is written in terms of the pressure P , the energy density ρ , and the electric charge density σ . An expression for these magnitudes can be obtained by assuming that we have a large number of particles within one AdS radius in the $mL \gg 1$ limit, by making use of the Thomas-Fermi approximation

$$\begin{aligned} P &= \frac{g}{24\pi^3} \int d^3 p F(\vec{p}) \frac{\vec{p}^2}{\sqrt{\vec{p}^2 + m^2}} \\ \rho &= \frac{g}{8\pi^3} \int d^3 p F(\vec{p}) \sqrt{\vec{p}^2 + m^2} \\ \sigma &= \frac{g}{8\pi^3} \int d^3 p F(\vec{p}) \end{aligned} \quad (2.3)$$

where g is the number of particle species and $F(p)$ is the Fermi-Dirac distribution function

$$F(\vec{p}) = \frac{1}{e^{\frac{\sqrt{\vec{p}^2 + m^2} - \mu}{T}} + 1} \quad (2.4)$$

written in terms of the local temperature T and chemical potential μ .

We use an static and spherically symmetric Ansatz for the background fields, as follows

$$\begin{aligned} A &= \frac{eL}{\kappa} h dt & u &= u^0 \partial_t \\ ds^2 &= L^2 (-f dt^2 + g dr^2 + r^2 d\Omega_2^2) \end{aligned} \quad (2.5)$$

where $d\Omega_2^2$ is the metric of the two-sphere, and f, g and h are functions of the radial coordinate r . The multiplicative constants in the gauge field Ansatz have been chosen for

later convenience. The four-velocity must satisfy the timelike condition $g_{\mu\nu}u^\nu u^\mu = -1$ which result in $u^0 = 1/L\sqrt{f}$.

In what follows, we find convenient to parametrize the Ansatz functions as

$$f = e^\chi \left(1 - \frac{2M}{r} + \frac{Q^2}{2r^2} + r^2 \right) \quad (2.6)$$

$$g = \left(1 - \frac{2M}{r} + \frac{Q^2}{2r^2} + r^2 \right)^{-1} \quad (2.7)$$

In terms of the new functions M, χ and Q of the radial coordinate r , where Q is the conserved local charge due to the $U(1)$ symmetry [25]

$$Q = e^{-\frac{\chi}{2}} r^2 h' \quad (2.8)$$

Also, we identify the local electric field as

$$E = \sqrt{g^{tt}} \sqrt{g^{rr}} F_{rt} = e^{-\frac{\chi}{2}} h' \quad (2.9)$$

In terms of the new functions, the equations of motion of the system read

$$\chi' = rg(\tilde{P} + \tilde{\rho}) \quad (2.10)$$

$$E' = -2 \frac{E}{r} + \sqrt{g} \tilde{\sigma} \quad (2.11)$$

$$M' = \frac{r^2}{2} (\tilde{\rho} + r E \sqrt{g} \tilde{\sigma}) \quad (2.12)$$

$$\tilde{P}' = 2 \frac{E^2}{r} + E E' + \frac{\chi' (g' - g \chi')}{2 r g^2} \quad (2.13)$$

where the last equation comes from the conservation of the energy-momentum tensor, and we rescaled

$$\rho = \frac{\tilde{\rho}}{L^2 \kappa^2} \quad , \quad P = \frac{\tilde{P}}{L^2 \kappa^2} \quad , \quad \sigma = \frac{\tilde{\sigma}}{L^2 e \kappa} \quad (2.14)$$

We consider the limit $mL \gg 1$, corresponding to a regime with a large number of particles within the AdS curvature radius. In this limit, the dimensionless energy density $\tilde{\rho}$, pressure \tilde{P} , and charge density $\tilde{\sigma}$ are derived from the statistics of a large ensemble of charged fermions in thermodynamic equilibrium.

In the context of finite-temperature field theory, the system is described by a grand canonical ensemble where particles and antiparticles constitute distinct thermal excitations within the Fock space [23]. Both species contribute additively to the energy density and pressure, whereas the charge density is determined by the net particle number (*i.e.*, the difference between particle and antiparticle populations) [24]. Consequently, the equations of state take the form

$$\begin{aligned} \rho &= \frac{g}{8\pi^3} \int (f(p, \mu) + f(p, \bar{\mu})) \sqrt{p^2 + m^2} d^3 p \\ P &= \frac{g}{8\pi^3} \int (f(p, \mu) + f(p, \bar{\mu})) \frac{p^2}{\sqrt{p^2 + m^2}} d^3 p \\ \sigma &= \frac{g}{8\pi^3} \int (f(p, \mu) - f(p, \bar{\mu})) d^3 p \end{aligned} \quad (2.15)$$

where $f(p, \mu)$ is the distribution function, and μ and $\bar{\mu}$ denote the particle and antiparticle chemical potentials, respectively. Here, we have assumed a particle charge of +1 (following the minimal coupling convention detailed in Appendix A).

Focusing on static and stable electron star configurations, we impose the equilibrium condition $\bar{\mu} = -\mu$. This condition implies a locally balanced creation and annihilation of particle-antiparticle pairs but does not imply symmetry in the number densities ($n \neq \bar{n}$) [26]. Instead, the system sustains a net conserved charge density σ determined by the value of μ . Substituting $\bar{\mu} = -\mu$, transforming to the dimensionless energy variable $\epsilon = E/m$, and rescaling according to Eq. (2.14), the equations of state yields

$$\begin{aligned}\tilde{\rho} &= \gamma \int_1^\infty (f(\epsilon, \mu) + f(\epsilon, -\mu)) \epsilon^2 \sqrt{\epsilon^2 - 1} d\epsilon \\ \tilde{P} &= \frac{\gamma}{3} \int_1^\infty (f(\epsilon, \mu) + f(\epsilon, -\mu)) (\epsilon^2 - 1)^{3/2} d\epsilon \\ \tilde{\sigma} &= \frac{\gamma}{\tilde{m}} \int_1^\infty (f(\epsilon, \mu) - f(\epsilon, -\mu)) \epsilon \sqrt{\epsilon^2 - 1} d\epsilon\end{aligned}\quad (2.16)$$

where we have defined $\gamma = gL^2\kappa^2m^4/(8\pi)^3$ and $\tilde{m} = m\kappa/e$. The function $f(\epsilon, \mu)$ is the Fermi-Dirac distribution

$$f(\epsilon, \mu) = \frac{1}{e^{\beta(\epsilon-\mu)} + 1} \quad (2.17)$$

where the local dimensionless inverse temperature $\beta = 1/T$ (setting $k_B = 1$) and the chemical potential μ are radial functions satisfying the thermodynamic equilibrium conditions.

Notice that we are working not only in the limit $mL \gg 1$ but also in the classical limit $\kappa^2/L^2 \ll 1$, and they are both in the definition of γ . However, as discussed in [8], we are interested in the scaled limit where $\gamma \sim 1$. This is obtained by taking $e^{-1} \sim \kappa/L \ll 1$, i.e. we require the gravitational coupling to be the square of the Maxwell coupling ('probe brane' limit). Furthermore, these limits implies for the scaled mass $\tilde{m}^2 \sim \sqrt{\gamma} \sim 1$.

Necessary and sufficient conditions for our charged perfect fluid to be in thermodynamic equilibrium are given by the Tolman and Klein relations when the particles are coupled to an external field (see details in Appendix A and [26, 27]))

$$T(r) = \frac{T_0}{\sqrt{f(r)}} \quad \& \quad \mu(r) = \frac{\mu_0 + h(r)}{\sqrt{f(r)}} \quad (2.18)$$

where T_0 and μ_0 are reference values. Note that with $h = 0$, we recover the already studied holographic neutron star conditions [12, 13].

We will solve now the equations of motions (2.10), satisfying the equations of state (2.16) in thermodynamic equilibrium (2.18). These equations of state are local and depend on r , thus we need to set some initial conditions at $r = 0$. We will start the construction imposing null conditions at the origin (which will lead to a BH), and then with some central values (a pure electron star configuration).

3 Solutions: black hole and electron star

Let us now solve the equations of motion (2.10) with specific central values for the equations of state (2.16). We begin by imposing the initial conditions $\tilde{\sigma} = \tilde{\rho} = \tilde{p} = 0$, which imply $\tilde{P}' = 0$. This condition means the absence of fluid not only at $r = 0$ but also throughout the radial coordinate; hence, it corresponds to the vacuum solution. By solving the remaining equations, we obtain

$$\chi = 0, \quad M = M_0, \quad Q = Q_0 \quad \& \quad h = -\frac{Q_0}{r} + \mu_{\text{BH}} \quad (3.1)$$

This yields the Reissner-Nordström AdS solution, where M_0 and Q_0 denote the black hole mass and charge, respectively, with a singularity at the origin $r = 0$. We also require the potential h to vanish at the horizon to avoid a conical singularity in the Euclidean continuation [21], thus $\mu_{\text{BH}} = Q_0/r_0$, with r_0 being the outer horizon.

Beyond the horizon, one might think a possible configuration consisting of a cloud of charged particles in equilibrium surrounding the black hole. This type of star configuration has been studied in [8, 10], where the temperature of the particle cloud is fixed at $T = 0$. Consequently, these constructions are not in thermodynamic equilibrium with the black hole. If we consider the cloud at a non-zero temperature and impose thermodynamic equilibrium with the black hole, we find that these configurations are not stable (at least at the classical level), as explained in Appendix C. In conclusion, for a thermal star with a black hole at the origin, the only thermodynamically stable configuration arises when all particles eventually fall into the black hole, resulting in a pure Reissner-Nordström black hole solution.

Alternatively, the equations of motion admit a regular vacuum solution known as Thermal AdS₄ (TAdS₄). This geometry is obtained by setting $M_0 = Q_0 = 0$ in Eq. (3.1) and fixing the gauge potential to a constant value, $h(r) = \mu_{\text{TAdS}}$, throughout the bulk. This solution represents a regular vacuum state with a constant chemical potential extending from the boundary to the origin.

Let us now consider the equations of motion (2.10) subject to specific initial conditions at the center of the star¹. We require the solution to be regular at the origin, implying

$$f(0) = 1 = g(0), \quad h(0) = 0, \quad T(0) = T_0 \quad (3.2)$$

By varying the central values T_0 and μ_0 , we numerically obtain the mass and charge profiles shown in Fig. 1. We observe that the star exhibits a well-defined boundary within the numerical radial cutoff, beyond which the star parameters saturate to constant values

$$M(r) \sim M_s, \quad Q(r) \sim Q_s, \quad \chi(r) \sim \chi_s \quad (3.3)$$

and the solution takes the asymptotic form

$$f(r) \sim e^{\chi_s} \left(1 - \frac{2M_s}{r} + \frac{Q_s^2}{2r^2} + r^2 \right) \quad \& \quad h(r) \sim -e^{\frac{\chi_s}{2}} \frac{Q_s}{r} + h_\infty \quad (3.4)$$

¹For the numerical integration, the differential equation for $P(r)$ is redundant, as the pressure is determined by the equation of state (2.16). Nevertheless, this equation serves as a consistent check for the local chemical potential $\mu(r)$ defined in (A.12).

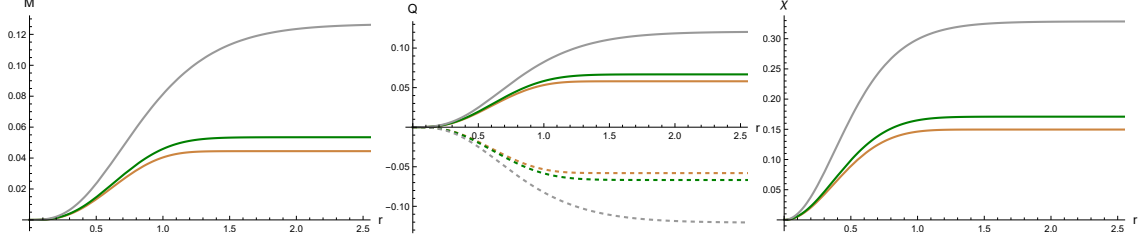


Figure 1. Radial profiles of the local mass $M(r)$, charge $Q(r)$, and metric function $\chi(r)$ for the Electron Star, obtained via the shooting method by varying the central parameters μ_0 and T_0 . The colors of the curves correspond to the specific points marked in the phase space diagram (Fig. 2). Solid lines represent solutions with positive central chemical potential μ_0 , while dashed lines correspond to $-\mu_0$ (with the same magnitude). Note that the mass and χ profiles coincide for both signs, illustrating the invariance of the geometry under charge conjugation.

Consequently, the metric at large r approaches the Reissner-Nordström solution with the time coordinate rescaled by a factor of $e^{\frac{\chi_s}{2}}$.

We are interested in the asymptotic thermodynamic values in order to compare our results with other solutions characterized by the same boundary temperature and chemical potential. Thus, we require the solution to approach pure AdS_4 at the boundary. Since the lapse function in (3.4) asymptotically approaches the AdS_4 form, eq. (2.18) yields

$$\mu \sim \frac{\mu_\infty}{\sqrt{1+r^2}} \quad \& \quad T \sim \frac{T_\infty}{\sqrt{1+r^2}} \quad (3.5)$$

where we defined

$$T_\infty = e^{-\frac{\chi_s}{2}} T_0 \quad \& \quad \mu_\infty = e^{-\frac{\chi_s}{2}} (\mu_0 + h_\infty) \quad (3.6)$$

We thus construct the star profiles in terms of T_∞ and μ_∞ by using the shooting method to map the central values T_0 and μ_0 to the boundary, as shown in Fig. 2. As evident from the figure, these profiles correspond exclusively to ‘pure core’ stars: we observe a region characterized by an ‘abrupt edge’. Subsequently, a power-law behavior emerges and evolves into a ‘cusp’ star. The appearance of the power law denotes a critical region where the star solution becomes unstable. Consequently, a stable solution exists only within the region delimited by the critical curve. As we increase the temperature or chemical potential beyond this boundary, the star collapses. The critical curve is constructed using the Katz criterion, where each critical point is identified by the vertical asymptote where the first derivative of the curve changes sign [18, 19]².

²The Katz criterion identifies a vertical asymptote in the caloric curve $-M_s(T_\infty^{-1})$ while keeping μ_∞/T_∞ fixed. This constraint ensures that we compare star solutions with the same entropy per particle $s = S/N$. In the neutron star case [14], this ratio is constant throughout the bulk, so fixing the central parameters μ_0/T_0 is equivalent to fixing the boundary values. In the present electron star case, however, the ratio varies radially. From (3.5), we have $\mu_\infty/T_\infty = (\mu_0 + h_\infty)/T_0$, where h_∞ is obtained numerically. Nevertheless, since h_∞ remains small up to the critical region (see Fig. 2), we approximate the Katz curves by fixing μ_0/T_0 . This approximation introduces a discrepancy of $\sim 15\%$ between the critical central and boundary values. This instability signals a second-order phase transition, which would occur well after the first-order transition discussed in Sec. 4.

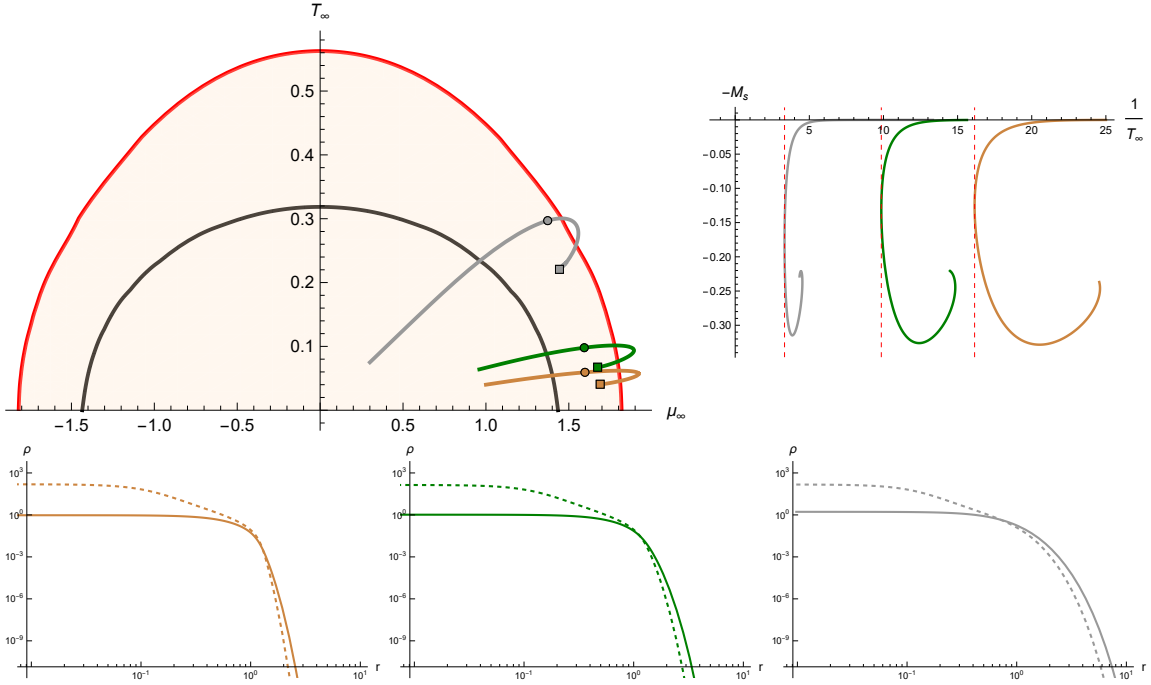


Figure 2. **Top:** (Left) The shaded region indicates the domain where the Electron Star is a stable solution according to the Katz criterion. This region is delimited by the red critical curve, which is constructed by varying the initial values μ_0 and T_0 and identifying the critical point on the corresponding Katz curve. The colored curves represent families of solutions with fixed μ_0/T_0 , where circles and squares denote representative stable and unstable configurations, respectively. The solid black line marks the star-black hole phase transition derived in Sec. 4. (Right) Katz stability curves for the families indicated in the phase diagram. The vertical dashed red lines mark the critical point obtained for each curve. **Bottom:** Log-Log plot for the radial density profiles corresponding to the specific configurations marked in the top-left panel; the colors match the phase space trajectories. Solid lines represent stable solutions (circles in the top-left figure), characterized by an abrupt edge profile, while dashed lines correspond to unstable solutions (squares) exhibiting power-law behavior.

Having identified the domain where the electron star solution exists, we must now determine its thermodynamic stability relative to the vacuum solutions, namely the Reissner-Nordström black hole and TAdS. To this end, in the following section, we will evaluate and compare the free energies of these geometries to construct the complete phase diagram of the system.

4 Phase Transitions

Let us now compute the free energy in the grand canonical ensemble for the different geometries obtained in the previous section. The free energy is obtained from the partition function via the relation

$$F = -T \log Z \quad (4.1)$$

The problem then reduces to computing the partition function from the gravitational path integral in Euclidean signature,

$$Z = \int Dg D\Phi e^{-S_E[g, \Phi]} \quad (4.2)$$

with

$$S_E[g, \Phi] = \frac{1}{2\kappa^2} \int \sqrt{g} (R[g] + \dots) + S_{\text{b.t.}} \quad (4.3)$$

and where Φ denotes all the matter fields and $S_{\text{b.t.}}$ the boundary terms. We work in the saddle point approximation, where the path integral is dominated by the classical gravity solutions, *i.e.* the on-shell configurations (we denote the Euclidean on-shell action by I). In this semiclassical approximation, we must sum over all relevant saddle points contributing to the path integral

$$Z_{\text{grav}} \approx e^{-I^{(\text{Star})}} + e^{-I^{(\text{BH})}} + e^{-I^{(\text{TAdS})}} \quad (4.4)$$

The details of each Euclidean on-shell action computation are provided in Appendix B. Notice that since the action is of order $1/\kappa^2$ (which is large in the classical limit), the partition function is exponentially dominated by the term with the smallest action (*i.e.* the minimum free energy). As explained in the Appendix, we defined the temperature and chemical potential in the previous section ensuring that all three saddle points share the same boundary values T_∞ and μ_∞ . Thus, by expressing the actions in terms of T_∞ and μ_∞ , we map the phase space and determine the dominant phase. The resulting free energies to be compared are given by

$$\begin{aligned} F^{(\text{BH})} &= \frac{\pi}{27} \left(2\pi T_\infty - \sqrt{2} \sqrt{3\mu_\infty^2 + 8\pi^2 T_\infty^2 - 6} \right) \left(\sqrt{2} \sqrt{3\mu_\infty^2 + 8\pi^2 T_\infty^2 - 6} + 4\pi T_\infty \right)^2 \\ F^{(\text{TAdS})} &= 0 \\ F^{(\text{Star})} &= 4\pi e^{\frac{X_s}{2}} (2M_s - Q_s \mu_\infty) - T_\infty S_s \end{aligned} \quad (4.5)$$

where we take $\kappa^2 \rightarrow 1$ and $L^2 \rightarrow 1$, and S_s is the electron star entropy computed in Appendix B. Notice that these free energies are symmetric under $\mu_\infty \leftrightarrow -\mu_\infty$ (as expected for a relativistic fluid of fermions, where the equation of state (2.16) shares this symmetry); we will thus focus on the $\mu_\infty \geq 0$ sector of the phase diagram.

We analyze the electron star profiles obtained in the previous section and compare their free energy at each point (μ_∞, T_∞) with those of the competing saddles. This construction is shown in Fig. 3, where we identify the regions of dominance corresponding to the minimal free energy. It is important to remark that we evaluated the free energies within the thermodynamic domain bounded by the star's critical curve (see Fig. 2). Consequently,

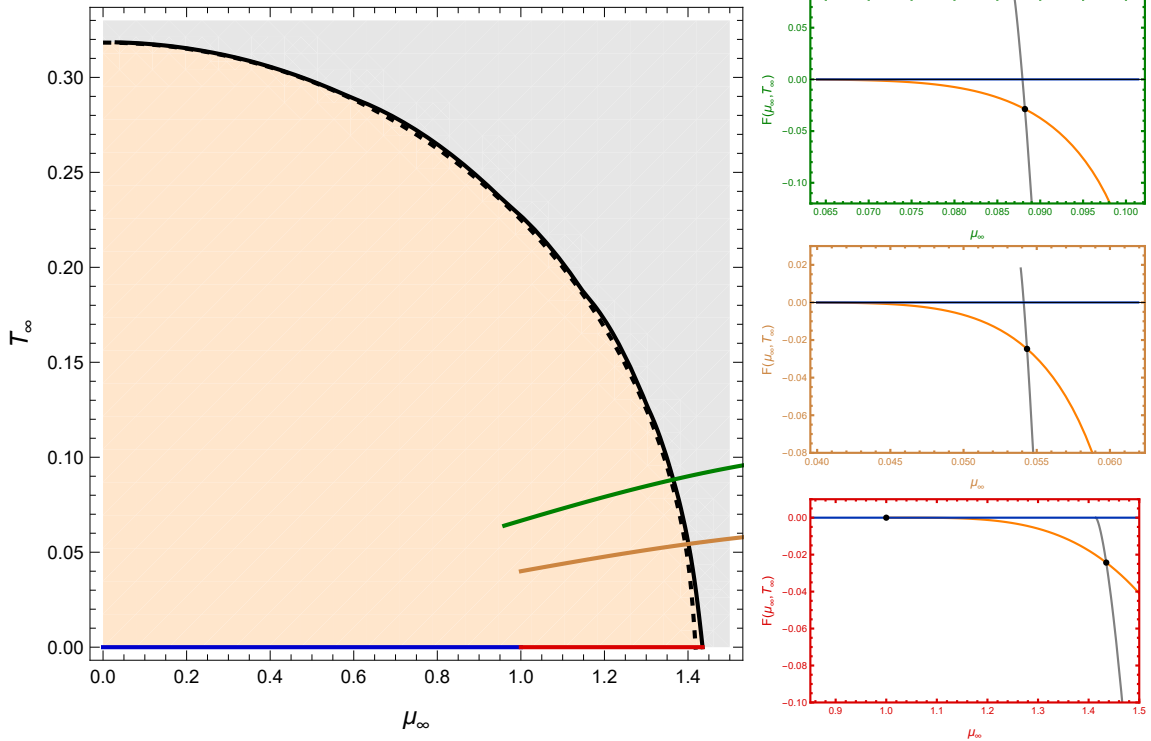


Figure 3. Left: Phase diagram of the holographic electron star in the boundary plane (μ_∞, T_∞) . The colored region indicates where the electron star is the dominant solution (minimal free energy), while the blue line and grey region correspond to TAdS and black hole dominance, respectively. The solid black lines denote first-order phase transition, and the dashed black line indicates where the Hawking-Page transition would occur in the absence of the star [22]. The colored lines (green, brown, red) represent the slices along which we evaluate the free energies shown in the right panels. **Right:** Free energy comparisons for the electron star (orange), black hole (grey), and TAdS (blue) corresponding to the cuts in the phase diagram. The frame colors match the cuts in the left panel. The black dots mark the phase transition points. The red frame corresponds to the $T_\infty = 0$ case, from which the quantum critical point is determined.

while the star solution technically exists in regions overlapping with the TAdS and black hole phases, the star phase is dominant only within a bounded region preceding its collapse.

From the constructed phase diagram in Fig. 3, we observe sharp boundaries where the dominance switches between solutions, indicating first-order phase transitions. We find that at finite temperatures, the two dominant phases are the electron star and the black hole, with a phase transition occurring at $I^{(\text{Star})} = I^{(\text{BH})}$. In contrast, at zero temperature, the TAdS region emerges, giving rise to TAdS₄-star and star-BH phase transitions. We compare the star-BH boundary with the Hawking-Page phase transition between TAdS₄ and a charged black hole [22], where the dotted line corresponds to the condition $I^{(\text{TAdS})} = I^{(\text{BH})}$.

Quantum critical point. We treat the zero-temperature case separately to explicitly compute the quantum critical point. This limit has been studied in the literature [11]; the equations of motion (2.10) remain unchanged, but the Fermi-Dirac distribution becomes a Heaviside step function. Focusing on the $\mu > 0$ case (there are only particles), the

equations of state become

$$\tilde{\rho} = \gamma \int_1^\mu \epsilon^2 \sqrt{\epsilon^2 - 1} \, d\epsilon, \quad \tilde{\sigma} = \frac{\gamma}{\tilde{m}} \int_1^\mu \epsilon \sqrt{\epsilon^2 - 1} \, d\epsilon \quad \& \quad \tilde{P} = \mu \tilde{\sigma} - \tilde{\rho} \quad (4.6)$$

Using the shooting method to map the central chemical potential μ_0 to the boundary value μ_∞ , we compute the free energies (4.5). This correspond to $T_\infty = 0$ in Fig. 3, and agrees with the non-null temperature results in the figure.

Since the local chemical potential decreases with r , a star profile can only exist if the central potential satisfies $\mu_0 \geq 1$. The limiting case $\mu_0 = 1$ (which also corresponds to the boundary value $\mu_\infty = 1$) represents the first point in Fig. 3, marking the transition from TAdS4 to the Electron Star geometry. As μ_∞ increases, we approach the black hole solution domain. In our regularization convention (4.5), the standard Hawking-Page critical point occurs at $\mu_\infty = \sqrt{2}$. However, our numerical results indicate that the quantum critical point marking the transition from the dominant electron star phase to the black hole phase occurs after the Hawking-Page point, specifically at $\mu_\infty \approx 1.435$.

5 Discussion and future directions

We have constructed the spherically symmetric holographic electron star solution at finite temperature T and chemical potential μ . We performed a Katz equilibrium analysis and found that the system possesses a stable branch that eventually destabilizes at a certain temperature, never regaining stability. This implies the existence of a finite region in the boundary phase space (μ_∞, T_∞) where the star is stable, extending up to a critical boundary where a second-order phase transition occurs. Contrary to the neutron star case previously studied in [12], the electron star only exhibits a dense core structure when it is stable, while the power-law behavior emerges strictly when the solution becomes unstable.

We computed the free energy of the star in the grand canonical ensemble and compared it with the Reissner-Nordström black hole and TAdS4 vacuum solutions within the saddle point approximation. At finite temperature, the dominant solutions are the electron star and the black hole, for which we obtained the corresponding phase transition curve. Notably, this first-order phase transition occurs well before the aforementioned second-order instability. We interpret the resulting phase diagram as corresponding to a holographic metal at finite density. Furthermore, we identified a quantum critical point at finite chemical potential, around which the different phases are organized.

Interestingly, the star-BH transition curve is qualitatively similar to the Hawking-Page curve obtained for the TAdS-BH vacuum phase transition [22]. In the standard Hawking-Page scenario, this curve signals a confinement/deconfinement transition. In our case, we found another saddle point solution that dominates over TAdS and could serve as a novel background for constructing spherically symmetric holographic superconductors [1].

A natural extension of this research would be to compute the bosonic and fermionic correlators on this background. As has already been done for the neutron star [31, 32], such an analysis is expected to exhibit rich holographic properties.

6 Acknowledgements

This work was partially supported by CONICET grant PIP-2023-11220220100262CO, and UNLP grant 2022-11/X931. The authors are grateful to Pablo Pisani, Adrián Lugo, Tobías Canavesi, Valentina Crespi, Carlos Argüelles and Octavio Fierro for discussions on various subjects related to the present manuscript. L.A. thanks ICTP for hospitality and support during this work.

A Details of the model

We aim to describe the thermodynamics of a large number of charged self-gravitating fermions in equilibrium (also known as ‘Electron Stars’) within a holographic framework. To this end, we consider a 3+1 dimensional global AdS spacetime and approximate the matter dynamics as a charged perfect fluid coupled to the gravitational field. The action functional consists of three contributions: the Einstein-Hilbert ($S_{\text{Eins.}}$), Maxwell ($S_{\text{Mxwl.}}$), and ideal fluid (S_{Fluid}) terms

$$S = \int d^4x \sqrt{-g} (\mathcal{L}_{\text{Eins.}} + \mathcal{L}_{\text{Mxwl.}} + \mathcal{L}_{\text{Fluid}}) \quad (\text{A.1})$$

where

$$\mathcal{L}_{\text{Eins.}} = \frac{1}{2\kappa^2} \left(R + \frac{6}{L^2} \right) \quad (\text{A.2})$$

$$\mathcal{L}_{\text{Mxwl.}} = -\frac{1}{4e^2} F_{\mu\nu} F^{\mu\nu} \quad (\text{A.3})$$

$$\mathcal{L}_{\text{Fluid}} = -\rho(\sigma, s) + \sigma u^\mu (\partial_\mu \phi + \theta \partial_\mu s + A_\mu) + \lambda(u^\mu u_\mu + 1) \quad (\text{A.4})$$

We employ natural units ($\hbar = c = k_B = 1$) and set the fermion charge to unity. The fluid sector follows the Schutz formalism [28]. Here, u^μ , ρ , σ , and s denote the four-velocity, energy density, charge density, and entropy per particle of the fluid, respectively. Furthermore, λ and θ are Lagrange multipliers, ϕ is a ‘Clebsch’ potential associated with the fluid velocity, and A_μ is the gauge potential (consequently, ϕ must shift under a gauge transformation to preserve gauge invariance).

The equations of motion are obtained by taking functional variations of the action. Focusing on the fluid sector, variations with respect to $\delta\lambda$, $\delta\sigma$, δs , $\delta\theta$, and $\delta\phi$ yield

$$u^\mu u_\mu = -1 \quad (\text{A.5})$$

$$\frac{\partial \rho(\sigma, s)}{\partial \sigma} = u^\mu (\partial_\mu \phi + \theta \partial_\mu s + A_\mu) \quad (\text{A.6})$$

$$\frac{\partial \rho(\sigma, s)}{\partial s} = -\nabla_\mu (u^\mu \sigma \theta) \quad (\text{A.7})$$

$$\sigma u^\mu \partial_\mu s = 0 \quad (\text{A.8})$$

$$\nabla_\mu (\sigma u^\mu) = 0 \quad (\text{A.9})$$

The first equation enforces the timelike normalization of the fluid velocity. If we identify the local chemical potential as

$$\mu \equiv \frac{\partial \rho(\sigma, \theta)}{\partial \sigma} \quad (\text{A.10})$$

Eq. (A.6) can be rewritten as

$$\mu = u^\mu (\partial_\mu \phi + A_\mu) \quad (\text{A.11})$$

where we used the entropy conservation condition (A.8) (characteristic of an adiabatic fluid) to eliminate the $u^\mu \partial_\mu s$ term. Notice that the chemical potential is gauge invariant

and consists of the baryonic conservation term, $u^\mu \partial_\mu \phi$, plus the coupling to the gauge field, $u^\mu A_\mu$. For the Ansatz introduced in Sec. 2, the local chemical potential reads

$$\mu = \sqrt{g^{00}} \left(\mu_0 + \frac{\kappa}{L e} A_t \right) = \frac{\mu_0 + h}{\sqrt{f}} \quad (\text{A.12})$$

where we have rescaled the variables to define a dimensionless chemical potential. Thus, μ comprises the constant chemical potential μ_0 (associated with the particle number) and the local value of the background Maxwell field.

Additionally, Eq. (A.9) represents the continuity equation for the fluid current vector J^μ if we identify

$$J^\mu \equiv \sigma u^\mu \quad (\text{A.13})$$

This implies that (A.8) becomes the continuity equation for the total entropy, $\nabla_\mu (u^\mu \sigma s) = 0$. Moreover, identifying the local temperature as

$$\frac{\partial \rho}{\partial s} \equiv \sigma T \quad (\text{A.14})$$

and utilizing the continuity equation (A.9), Eq. (A.7) simplifies to

$$T = -u^\mu \partial_\mu \theta \quad (\text{A.15})$$

Next, varying the action with respect to δu^μ leads to

$$\sigma (\partial_\mu \phi + \theta \partial_\mu s + A_\mu) + 2\lambda u_\mu = 0 \quad (\text{A.16})$$

Contracting this equation with u^μ and using the previous results allows us to determine the Lagrange multiplier λ

$$\lambda = \frac{\sigma u^\mu (\partial_\mu \phi + \theta \partial_\mu s + A_\mu)}{2} = \frac{\sigma \mu}{2} \quad (\text{A.17})$$

On the other hand, varying the action with respect to the gauge potential δA_μ yields the Maxwell equations

$$\nabla_\mu F^{\nu\mu} = e^2 J^\nu \quad (\text{A.18})$$

Finally, the variation with respect to the metric $\delta g_{\mu\nu}$ produces the Einstein equations with a negative cosmological constant $\Lambda = -3/L^2$, sourced by the energy-momentum tensors of the Maxwell field and the fluid

$$R^{\mu\nu} - \frac{1}{2} g^{\mu\nu} R - \frac{3}{L^2} g^{\mu\nu} = \kappa^2 (T_{\text{Mxwl.}}^{\mu\nu} + T_{\text{Fluid}}^{\mu\nu}) \quad (\text{A.19})$$

where the energy-momentum tensors are derived from the Lagrangians as

$$\begin{aligned} T_{\text{Fluid}}^{\mu\nu} &= g^{\mu\nu} P + (\rho + P) u^\mu u^\nu \\ T_{\text{Mxwl.}}^{\mu\nu} &= \frac{1}{e^2} \left(F^{\mu\alpha} F_\alpha^\nu - \frac{1}{4} g^{\mu\nu} F_{\alpha\beta} F^{\alpha\beta} \right) \end{aligned} \quad (\text{A.20})$$

We have thus derived the equations of motion for the model (A.1), which were introduced in Sec. 2 and solved in Sec. 3 to obtain the Electron Star and vacuum solutions (Black Hole and TAdS).

As a result, we observe that the fluid sector of the action (A.4) can be evaluated on-shell immediately by employing Eqs. (A.5) and (A.11),

$$\mathcal{L}_{\text{Fluid}}^{\text{on-shell}} = -\rho + \mu\sigma \quad (\text{A.21})$$

Furthermore, from the local Gibbs-Duhem relation $P + \rho = \mu\sigma + TS$, which remains locally valid in curved spacetime [20], we obtain

$$\mathcal{L}_{\text{Fluid}}^{\text{on-shell}} = P - TS \quad (\text{A.22})$$

with $S = s\sigma$ the local entropy density of the star. Notice that this is not the expected result for the variational principle of the Schutz model, as it differs by the TS term. This term corresponds to a total derivative, $\nabla_\mu(\sigma\theta u^\mu s) = -TS$; thus, it does not affect the equations of motion but defines the boundary condition of the ensemble [29], which will be important when computing the free energy in Appendix B.

B Free energy computation details

In this appendix, we compute the on-shell action required for the free energy analysis presented in Sec. 4. Since we compare saddle points sharing the same asymptotic symmetries, we first define the general procedure to compute the Euclidean on-shell action and subsequently apply it to each specific geometry. By performing a Wick rotation $t \rightarrow -i t_E$ on the Einstein action (A.1), with the Euclidean time periodicity $t_E \sim t_E + \beta$ (where $\beta = 1/T$), we obtain

$$I = - \int d^4x \sqrt{g} \mathcal{L}_{\text{bulk}} + I_{\text{GHY}} + I_{\text{ct}} \quad (\text{B.1})$$

where I_{ct} is the counterterm action required for asymptotically AdS_4 spaces [15],

$$I_{\text{ct}} = \frac{1}{\kappa^2} \int d^3x \frac{2}{L} \sqrt{\gamma} \left(1 + \frac{L^2}{4} R[\gamma] \right) \quad (\text{B.2})$$

Here, $R[\gamma]$ is the Ricci scalar of the boundary metric γ defined at the boundary hypersurface. On the other hand, I_{GHY} denotes the Gibbons-Hawking-York boundary term [16, 17],

$$I_{\text{GHY}} = - \frac{1}{\kappa^2} \int d^3x \sqrt{\gamma} K \quad (\text{B.3})$$

The geometries of interest share the same asymptotic symmetries; thus, we can define the boundary terms generally and then compute them explicitly for each solution. We first define the unit normal vector n^μ to the hypersurface ∂M at a constant cutoff $r = \Lambda$,

$$n_\mu = \frac{\delta_\mu^r}{\sqrt{g^{rr}}} \quad (\text{B.4})$$

where we have chosen the GH convention and defined the outgoing normal vector to the hypersurface. Then, the induced metric $\gamma_{\mu\nu}$ on the hypersurface ∂M (the projection tensor) for a timelike unit normal vector n^μ is

$$\gamma_{\mu\nu} = g_{\mu\nu} - n_\mu n_\nu \quad (\text{B.5})$$

In our case, which involves static spherically symmetric metrics, the induced metric is simply g_{ij} where i, j run over the transverse directions. Finally, the extrinsic curvature $K_{\mu\nu}$ is given by the Lie derivative of the induced metric along the normal vector direction

$$K_{\mu\nu} = \frac{1}{2} \mathcal{L}_n \gamma_{\mu\nu} = \nabla_{(\mu} n_{\nu)} \quad \& \quad K = g^{\mu\nu} K_{\mu\nu} \quad (\text{B.6})$$

We are interested in comparing the free energies of different bulk geometries. To do so consistently, we must impose that they describe the same boundary spacetime at the same temperature. This is achieved by introducing a reference location at a cutoff $r = \Lambda$, where each system possesses a boundary thermal circle of the same proper length. The proper length of the thermal circle for a static observer along Euclidean time is defined as

$$\ell_{\text{th}}(r) = \int_0^{T^{-1}} \sqrt{g_{00}(r)} dt_E = T^{-1} \sqrt{g_{00}(r)} \quad (\text{B.7})$$

Thus, matching the thermal lengths at $r = \Lambda$, we require

$$\tilde{\ell}_{\text{th}}(\Lambda) = \ell_{\text{th}}(\Lambda) \implies \tilde{T}^{-1} \sqrt{\tilde{g}_{00}(\Lambda)} = T^{-1} \sqrt{g_{00}(\Lambda)} \quad (\text{B.8})$$

Analogously, we match the chemical potentials. Since the chemical potential is defined as the gauge field component measured by a static observer, $u^\mu A_\mu = \mu$, we require the chemical potentials to coincide at the cutoff. In our framework, we have already defined the temperature and chemical potential such that, in the limit $\Lambda \rightarrow \infty$, we obtain

$$\mu_{\text{TAdS}} = \mu_{\text{BH}} = \mu_\infty \quad \& \quad T_{\text{TAdS}} = T_{\text{BH}} = T_\infty \quad (\text{B.9})$$

This ensures that the boundary conditions are identical for each solution. Consequently, we will express all quantities in terms of T_∞ and μ_∞ . It remains only to compute each free energy used in Sec. 4 to construct the phase diagram.

Black Hole. We consider the Euclidean version of the Ansatz (2.5) for the black hole solution (3.1), given by

$$f(r) = g(r)^{-1} = \left(1 - \frac{2M_0}{r} + \frac{Q_0^2}{2r^2} + r^2\right) \quad \& \quad h(r) = -\frac{Q_0}{r} + \mu_\infty \quad (\text{B.10})$$

The Hawking temperature is given by

$$T_\infty = \frac{f'(r_0)}{4\pi} \quad (\text{B.11})$$

where r_0 is the outer horizon radius. Recalling the gauge regularity condition $\mu_\infty = Q_0/r_0$, we can express the mass and charge in terms of T_∞ , μ_∞ , and r_0

$$Q_0 = \mu_\infty r_0 \quad \& \quad M_0 = \frac{r_0}{2} (\mu_\infty^2 + 4\pi r_0 T_\infty - 2r_0^2) \quad (\text{B.12})$$

Moreover, substituting these into the definition of the outer horizon, it turns out that for fixed temperature and chemical potential, there are two possible horizon radii

$$r_0^\pm = \frac{1}{6} \left(4\pi T_\infty \pm \sqrt{2} \sqrt{3\mu_\infty^2 + 8\pi^2 T_\infty^2 - 6} \right) \quad (\text{B.13})$$

These two branches, corresponding to the plus and minus signs, are referred to as the ‘large’ and ‘small’ black holes, respectively. Note that the existence of a physical horizon implies a constraint on T_∞ and μ_∞ ,

$$T \geq \frac{\sqrt{\frac{3}{2}(2 - \mu_\infty^2)}}{2\pi} \quad \text{and} \quad |\mu_\infty| \leq \sqrt{2}$$

or,

$$T \geq 0 \quad \text{and} \quad |\mu_\infty| > \sqrt{2} \quad (\text{only for large BH}) \quad (\text{B.14})$$

The latter condition arises from requiring $M_0 > 0$. Since we work in the Grand Canonical Ensemble, both solutions contribute to the path integral; therefore, we sum over all allowed saddle points.

Let us compute the Black Hole Euclidean on-shell action using a radial cutoff Λ

$$I_{\text{bulk}} = - \int_0^{\frac{1}{T_\infty}} dt_E \int d\Omega^2 \int_{r_0^\pm}^\Lambda dr \sqrt{g} \left(\frac{1}{2\kappa^2} \left(R + \frac{6}{L^2} \right) - \frac{1}{4e^2} F_{\mu\nu} F^{\mu\nu} \right) \quad (\text{B.15})$$

Using the on-shell relations $R = -12/L^2$ and $F^2 = -2e^2(\mu_\infty r_0^\pm)^2/(\kappa^2 L^2 r^4)$, we obtain

$$I_{\text{bulk}} = \frac{2\pi L^2}{\kappa^2 T_\infty} \left(2\Lambda^3 - r_0^\pm (2(r_0^\pm)^2 + \mu_\infty^2) + \mu_\infty^2 \frac{(r_0^\pm)^2}{\Lambda} \right) \quad (\text{B.16})$$

Notice that this term exhibits a cubic divergence $\mathcal{O}(\Lambda^3)$ as $\Lambda \rightarrow \infty$.

The GHY term evaluates to

$$I_{\text{GHY}} = \frac{2\pi L^2}{\kappa^2 T_\infty} \left(3r_0^\pm (\mu_\infty^2 - 2(r_0^\pm)^2 + 4\pi r_0^\pm T_\infty) - \mu_\infty^2 \frac{(r_0^\pm)^2}{\Lambda} - 4\Lambda - 6\Lambda^3 \right) \quad (\text{B.17})$$

This term contains divergences of order $\mathcal{O}(\Lambda^3)$ and $\mathcal{O}(\Lambda^1)$.

Finally, we compute the counterterm (B.2) to regularize the total action

$$\begin{aligned} I_{\text{ct}} &= \frac{2\pi L^2}{\kappa^2 T_\infty} \frac{(2\Lambda^2 + 1)}{\Lambda} \sqrt{4\Lambda (\Lambda^3 + \Lambda + 2(r_0^\pm)^3 - \mu_\infty^2 r_0^\pm) + 2(r_0^\pm)^2 (\mu_\infty^2 - 8\pi \Lambda T_\infty)} \\ &\approx \frac{4\pi L^2}{\kappa^2 T_\infty} (2\Lambda^3 + 2\Lambda + r_0^\pm (2(r_0^\pm)^2 - 4\pi r_0^\pm T_\infty - \mu_\infty^2)) + \mathcal{O}(\Lambda^{-1}) \end{aligned} \quad (\text{B.18})$$

All divergences cancel out exactly when combining these terms. Thus, taking the limit $\Lambda \rightarrow \infty$, the total regularized action is

$$I_{\text{BH}}^\pm = \frac{8\pi L^2}{\kappa^2 T_\infty} (r_0^\pm)^2 (\pi T_\infty - r_0^\pm) \quad (\text{B.19})$$

Since $r_0^+ \geq r_0^-$, it follows that

$$I_{\text{BH}}^+ \leq I_{\text{BH}}^- \quad (\text{B.20})$$

Consequently, the free energy of the large black hole is always lower than that of the small black hole, making it the dominant contribution. For the construction of the phase diagram, we will consider only the large black hole branch. Its free energy is given by (4.5).

Thermal AdS₄. The TAdS free energy is obtained immediately by taking the limit $M_0 = Q_0 = 0$ (implying $r_0 = 0$) in the black hole calculation. This yields $F_{\text{TAdS}} = 0$ for all T_∞ and μ_∞ . Comparing the TAdS free energy with that of the charged black hole leads to the Hawking-Page phase transition curve [22].

Electron Star. The details of the Electron Star model are provided in Appendix A. The Euclidean action is given by

$$I_{\text{bulk}} = - \int d^4x \sqrt{g} \left(\frac{1}{2\kappa^2} \left(R + \frac{6}{L^2} \right) - \frac{1}{4e^2} F_{\mu\nu} F^{\mu\nu} + \frac{\mu \tilde{\sigma} - \tilde{\rho}}{\kappa^2 L^2} \right) \quad (\text{B.21})$$

where the fluid term has already been evaluated on-shell using (A.21). Upon substituting the equations of motion (2.10), the integrand reduces entirely to a total derivative. Since

the star solution is required to be regular at the origin (as detailed in Sec. 2), the action reduces to a boundary term at the cutoff Λ ,

$$I_{\text{bulk}} = \frac{2\pi L^2}{\kappa^2 T_\infty} \Omega^2 e^{-\frac{\chi(\Omega)}{2}} (f'(\Omega) - 2h'(\Omega)(\mu_0 + h(\Omega))) \quad (\text{B.22})$$

Next, we compute the GHY term

$$I_{GHY} = -\frac{2\pi L^2}{\kappa^2 T_\infty} e^{-\frac{\chi(\Lambda)}{2}} \Lambda (\Lambda f'(\Lambda) + 4f(\Lambda)) \quad (\text{B.23})$$

Finally, the counterterm contribution (B.2) is

$$I_{\text{ct}} = \frac{4\pi L^2}{\kappa^2 T_\infty} (2\Lambda^2 + 1) f(\Lambda)^{\frac{1}{2}} \quad (\text{B.24})$$

Combining these contributions, taking the cutoff $\Lambda \rightarrow \infty$, and using the asymptotic form of the metric (3.4), the regularized Euclidean action yields

$$I^{(\text{Star})} = \frac{4\pi L^2}{\kappa^2 T_\infty} e^{\frac{\chi_s}{2}} (2M_s - \mu_\infty Q_s) \quad (\text{B.25})$$

From the discussion in the Appendix A, this action yields the thermodynamic potential associated with the adiabatic constraints of the fluid. To recover the Grand Canonical Potential F , we must correct the boundary term, which is just a Legendre transformation relating to entropy:

$$F = T_\infty I^{(\text{Star})} - T_\infty S_s \quad (\text{B.26})$$

where S_s is the total entropy of the star [10]. This correction is only need for the Electron Star since the entropic origin is different: the on-shell black hole action gives correctly the free energy since it entropy comes from the horizon; while in the star the geometric part has zero entropy, thus it can only comes from the star which we first computed for a adiabatic fluid and then transform back. The entropy can be computed integrating spatially the entropy density [30], which using the Gibbs-Duhem relation combined with the local temperature and chemical potential satisfying the equilibrium condition (2.18), yields

$$S_s = 4\pi \int_0^\infty dr \sqrt{g} r^2 S = 4\pi \int_0^\infty dr r^2 \left(e^{\frac{\chi}{2}} \frac{(\rho + P)}{T_0} - \sqrt{g} \frac{(\mu_0 + h)}{T_0} \sigma \right) \quad (\text{B.27})$$

This concludes the derivation of the free energies for the three classical geometries used in (4.5) to construct the complete phase diagram in Sec. 4.

C Black hole surrounded by an electron cloud

In this appendix, we analyze a Reissner-Nordström black hole surrounded by a gas of charged particles, referred to as an *electron cloud*. This type of configuration has been studied at zero temperature in [8], and with temperature effects in [10]. However, in the latter cases, the cloud is not in thermodynamic equilibrium with the black hole but is instead fixed at a background temperature of $T = 0$. We argue here that introducing a finite temperature to construct an electron cloud in full thermodynamic equilibrium with the black hole is not possible within this framework.

We obtained the black hole solution in Sec. 3. From the regularity conditions, the black hole temperature and gauge potential are given by

$$T_{\text{BH}} = \frac{f'(r_0)}{4\pi} \quad \& \quad h(r) = -\frac{Q_0}{r} + \mu_{\text{BH}} \quad (\text{C.1})$$

where $\mu_{\text{BH}} = Q_0/r_0$, r_0 is the outer horizon radius, and $f(r)$ and $h(r)$ are the black hole metric functions (3.1). On the other hand, the particle cloud is treated as a perfect fluid following the model introduced in Appendix A. Due to the spherical symmetry of the black hole, the cloud must respect this symmetry. A necessary and sufficient condition for the fluid to be in global thermal equilibrium is that it satisfies the local Tolman and gauge conditions

$$T(r) = \frac{T_0}{\sqrt{f(r)}} \quad \& \quad \mu(r) = \frac{\mu_0 + h(r)}{\sqrt{f(r)}} \quad (\text{C.2})$$

where T_0 and μ_0 are the initial conditions for the cloud. We use these conditions to solve the equations of state numerically. For simplicity, we focus the analysis on the Fermi-Dirac integrals of the form

$$\mathcal{I} = \int_1^\infty \frac{H(\epsilon)}{e^{\frac{(\epsilon-\mu)}{T}} + 1} d\epsilon \quad (\text{C.3})$$

where $H(\epsilon)$ represents the density of states function appearing in the definitions of ρ , σ , and P in (2.16).

If we attempt to construct a thermodynamically stable solution for a cloud extending to the black hole horizon, a divergence arises. Specifically, performing a Sommerfeld expansion at low temperatures (see Appendix E in [33]), we obtain

$$\mathcal{I} \approx \int_1^\mu H(\epsilon) d\epsilon + \frac{\pi^2}{6} T^2 H'(\mu) + \mathcal{O}(T^4) \quad (\text{C.4})$$

The first term corresponds to the zero-temperature limit (fully degenerate cloud). The issue arises with the finite-temperature corrections: if we impose equilibrium with the black hole, $T_0 = T_{\text{BH}}$, then the local temperature $T(r)$ diverges as $r \rightarrow r_0$ (since $f(r_0) = 0$). Consequently, the fluid density and pressure would diverge at the horizon. The only consistent solution in this setup is to set $T_0 = 0$, *i.e.*, the electron cloud must be at zero temperature. In this scenario, the fluid density vanishes at the horizon and the cloud only exists in regions where the local chemical potential satisfies $\mu(r) \geq 1$. This results in a black hole surrounded by a zero-temperature cloud, potentially with a global temperature parameter shifted by gravitational backreaction, but not in thermal contact with the horizon [10].

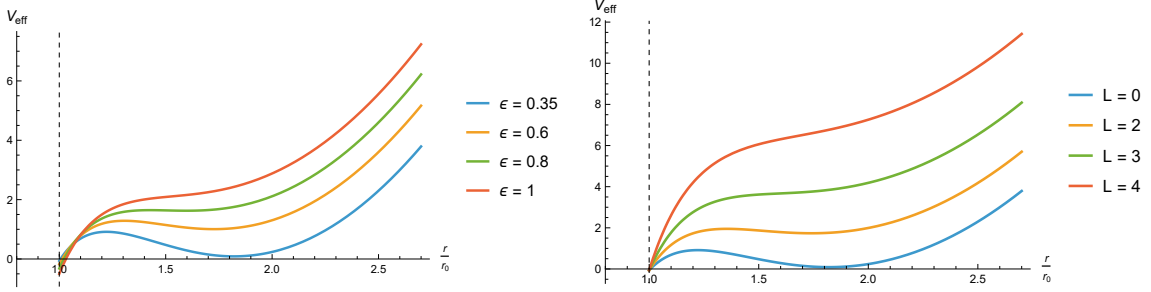


Figure 4. Plots of the effective potential (C.5), fixing the angular momentum $L = 0$ (Left) and the energy $\epsilon = 0.35$ (Right). Both plots have the horizon fixed (black dash line) at $M = 10$ and $Q = 4.5$. Plots of the effective potential (C.5). **Left:** Fixed angular momentum $L = 0$ with varying energy. **Right:** Fixed energy $\epsilon = 0.35$ with varying angular momentum. Both plots assume a fixed background with horizon radius corresponding to $M = 10$ and $Q = 4.5$, and the charge and mass of the particle are $q = 1$ and $m = 0.2$ respectively.

While static thermal equilibrium is forbidden, dynamically stable geodesics exist. The timelike condition $g_{\mu\nu}\dot{x}^\mu\dot{x}^\nu = -1$ together with the constants of motion implies $\frac{1}{2}\dot{r}^2 - V_{\text{eff}}(r) = 0$, with the effective potential [36]

$$V_{\text{eff}}(r) = \frac{f(r)}{2} \left(1 + \frac{L^2}{2}\right) - \frac{1}{2} \left(\epsilon + \frac{q}{m} h(r)\right)^2 \quad (\text{C.5})$$

with q , m and L being the charge, mass and angular momentum of the particle. Note that this potential depends on the energy ϵ and cannot be decoupled; allowed trajectories must satisfy $V_{\text{eff}}(r) \geq 0$. As shown in Fig. 4, the potential possesses stable minima. If a particle remains at the corresponding energy, the dynamics are stable; statistically, this corresponds to a zero-temperature cloud. However, introducing a finite temperature implies thermal fluctuations. These fluctuations allow particles in stable orbits to gain energy, overcome the potential barrier, and eventually fall into the horizon. This process continues until the cloud is depleted or reaches a fully degenerate ($T = 0$) state.

In conclusion, an electron cloud can only be considered at zero temperature and cannot coexist in thermal equilibrium with a finite-temperature black hole in this formalism. This is consistent with the fact that the equations of state used for the electron star assume a vacuum state where the absence of particles corresponds to zero temperature (Boulware vacuum); consequently, the horizon is a fixed boundary with no radiation. The divergence at the horizon could be regularized using a Hartle-Hawking vacuum, which defines thermodynamic equilibrium including Hawking radiation [34]. In that case, the horizon is dynamic and could exchange heat with the cloud. However, since we are interested in holographic applications, we restrict our analysis to the Boulware vacuum, as this corresponds to the ground state in the dual CFT, whereas the Hartle-Hawking vacuum corresponds to a thermal state in the dual theory [35].

References

- [1] S. A. Hartnoll, C. P. Herzog and G. T. Horowitz, *Building a Holographic Superconductor*, *Phys. Rev. Lett.* **101** (2008) 031601 [[arXiv:0803.3295](https://arxiv.org/abs/0803.3295)].
- [2] T. Faulkner, G. T. Horowitz, J. McGreevy, M. M. Roberts and D. Vegh, *Photoemission 'experiments' on holographic superconductors*, *JHEP* **03** (2010) 121 [[arXiv:0911.3402](https://arxiv.org/abs/0911.3402)].
- [3] S. S. Gubser, F. D. Rocha and P. Talavera, *Normalizable fermion modes in a holographic superconductor*, *JHEP* **10** (2010) 087 [[arXiv:0911.3632](https://arxiv.org/abs/0911.3632)].
- [4] S. A. Hartnoll, J. Polchinski, E. Silverstein and D. Tong, *Towards strange metallic holography*, *JHEP* **04** (2010) 120 [[arXiv:0912.1061](https://arxiv.org/abs/0912.1061)].
- [5] T. Faulkner, H. Liu, J. McGreevy and D. Vegh, *Emergent quantum criticality, Fermi surfaces, and AdS_2* , *Phys. Rev. D* **83** (2011) 125002 [[arXiv:0907.2694](https://arxiv.org/abs/0907.2694)].
- [6] M. Cubrovic, J. Zaanen and K. Schalm, *String Theory, Quantum Phase Transitions and the Emergent Fermi-Liquid*, *Science* **325** (2009) 439 [[arXiv:0904.1993](https://arxiv.org/abs/0904.1993)].
- [7] S. A. Hartnoll, D. M. Hofman and A. Tavanfar, *Holographically smeared Fermi surface: Quantum oscillations and Luttinger count in electron stars*, *Europhys. Lett.* **95** (2011) 31002 [[arXiv:1011.2502](https://arxiv.org/abs/1011.2502)].
- [8] S. A. Hartnoll and A. Tavanfar, *Electron stars for holographic metallic criticality*, *Phys. Rev. D* **83** (2011) 046003 [[arXiv:1008.2828](https://arxiv.org/abs/1008.2828)].
- [9] S. A. Hartnoll and P. Petrov, *Electron Star Birth: A Continuous Phase Transition at Nonzero Density*, *Phys. Rev. Lett.* **106** (2011) 121601 [[arXiv:1011.6469](https://arxiv.org/abs/1011.6469)].
- [10] V. G. M. Puletti, S. Nowling, L. Thorlacius and T. Zingg, *Holographic metals at finite temperature*, *JHEP* **01** (2011) 117 [[arXiv:1011.6261](https://arxiv.org/abs/1011.6261)].
- [11] X. Arsiwalla, J. de Boer, K. Papadodimas and E. Verlinde, *Degenerate Stars and Gravitational Collapse in AdS/CFT* , *JHEP* **01** (2011) 144 [[arXiv:1010.5784](https://arxiv.org/abs/1010.5784)].
- [12] C. A. Argüelles and N. Grandi, *Fermionic halos at finite temperature in AdS/CFT* , *JHEP* **05** (2018) 118 [[arXiv:1712.05866](https://arxiv.org/abs/1712.05866)].
- [13] C. A. Argüelles, E. Canavesi, M. Diaz and N. Grandi, *Thermodynamic instabilities in holographic neutron stars at finite temperature*, *Class. Quant. Grav.* **37** (2020) 205002 [[arXiv:1911.02554](https://arxiv.org/abs/1911.02554)].
- [14] E. Canavesi, *Holographic neutron stars at finite temperature*, [[arXiv:2312.10021](https://arxiv.org/abs/2312.10021)].
- [15] V. Balasubramanian and P. Kraus, *A stress tensor for Anti-de Sitter gravity*, *Commun. Math. Phys.* **208** (1999) 413 [[hep-th/9902121](https://arxiv.org/abs/hep-th/9902121)].
- [16] G. W. Gibbons and S. W. Hawking, *Action Integrals and Partition Functions in Quantum Gravity*, *Phys. Rev. D* **15** (1977) 2752.
- [17] J. W. York, Jr., *Role of conformal three-geometry in the dynamics of gravitation*, *Phys. Rev. Lett.* **28** (1972) 1082.
- [18] J. Katz, *On the number of unstable modes of an equilibrium*, *Mon. Not. Roy. Astron. Soc.* **183** (1978) 765.
- [19] J. Katz, *Thermodynamics and selfgravitating systems*, *Found. Phys.* **33** (2003) 223 [[astro-ph/0212295](https://arxiv.org/abs/astro-ph/0212295)].

[20] P.-H. Chavanis, *Statistical mechanics of self-gravitating systems in general relativity: I. The quantum Fermi gas*, *Eur. Phys. J. Plus* **135** (2020) 290 [[arXiv:1908.10806](https://arxiv.org/abs/1908.10806)].

[21] S. Kobayashi, D. Mateos, S. Matsuura, R. C. Myers and R. M. Thomson, *Holographic phase transitions at finite baryon density*, *JHEP* **02** (2007) 016 [[hep-th/0611099](https://arxiv.org/abs/hep-th/0611099)].

[22] A. Chamblin, R. Emparan, C. V. Johnson and R. C. Myers, *Charged AdS black holes and catastrophic holography*, *Phys. Rev. D* **60** (1999) 064018 [[hep-th/9902170](https://arxiv.org/abs/hep-th/9902170)].

[23] J. I. Kapusta and C. Gale, *Finite-temperature field theory: Principles and applications*, Cambridge University Press (2006).

[24] N. K. Glendenning, *Compact stars: Nuclear physics, particle physics, and general relativity*, Springer (1997).

[25] J. D. Bekenstein, *Hydrostatic Equilibrium and Gravitational Collapse of Relativistic Charged Fluid Balls*, *Phys. Rev. D* **4** (1971) 2185.

[26] L. D. Landau and E. M. Lifshitz, *Statistical Physics, Part 1*, Butterworth-Heinemann (1980).

[27] K. Shi, Y. Tian, X. Wu, H. Zhang and C. Zhu, *Thermodynamic equilibrium condition and the first law of thermodynamics for charged perfect fluids in electromagnetic and gravitational fields*, *Class. Quant. Grav.* **39** (2022) 085004 [[arXiv:2111.03816](https://arxiv.org/abs/2111.03816)].

[28] B. F. Schutz, *Perfect Fluids in General Relativity: Velocity Potentials and a Variational Principle*, *Phys. Rev. D* **2** (1970) 2762.

[29] J. D. Brown, *Action functionals for relativistic perfect fluids*, *Class. Quant. Grav.* **10** (1993) 1579 [[gr-qc/9304026](https://arxiv.org/abs/gr-qc/9304026)].

[30] P. H. Chavanis, *Relativistic stars with a linear equation of state: analogy with classical isothermal spheres and black holes*, *Astron. Astrophys.* **483** (2008) 673 [[arXiv:0707.2292](https://arxiv.org/abs/0707.2292)].

[31] E. Canavesi, O. Fierro, N. Grandi and P. Pisani, *Scalar correlators and normal modes in holographic neutron stars*, *Class. Quant. Grav.* **40** (2023) 025001 [[arXiv:2205.04374](https://arxiv.org/abs/2205.04374)].

[32] M. Acito, E. Canavesi, N. Grandi and A. Lugo, *Fermionic correlators on the holographic neutron star*, *JHEP* **04** (2024) 153 [[arXiv:2401.03362](https://arxiv.org/abs/2401.03362)].

[33] R. K. Pathria and P. D. Beale, *Statistical Mechanics*, 3rd ed., Elsevier (2011).

[34] P. Candelas, *Vacuum Polarization in Schwarzschild Spacetime*, *Phys. Rev. D* **21** (1980) 2185.

[35] E. Witten, *Anti-de Sitter space and holography*, *Adv. Theor. Math. Phys.* **2** (1998) 253 [[hep-th/9802150](https://arxiv.org/abs/hep-th/9802150)].

[36] M. Blau, *Lecture Notes on General Relativity*, University of Bern (2025), <http://www.blau.itp.unibe.ch/GRLectureNotes.html>.